Decoupling thermal and electrical transport in α -MgAgSb with synergic pressure and doping strategy

Cite as: J. Appl. Phys. **125**, 205105 (2019); doi: 10.1063/1.5090456 Submitted: 28 January 2019 · Accepted: 3 May 2019 · Published Online: 23 May 2019







Jia-Yue Yang,^{1,2} Wenjie Zhang,¹ and Ming Hu^{3,a)}

AFFILIATIONS

- ¹School of Energy and Power Engineering, Shandong University, Qingdao 266237, China
- ²Institute of Mineral Engineering, Division of Material Science and Engineering, RWTH Aachen University, Aachen 52064, Germany
- ³Department of Mechanical Engineering, University of South Carolina, Columbia, South Carolina 29208, USA

ABSTRACT

The Nowotny–Juza α -MgAgSb has been demonstrated to be a promising candidate for room-temperature thermoelectric material, owing to its ultralow lattice thermal conductivity. The challenge of enhancing its figure of merit (ZT) for commercial applications is how to effectively decouple the electrical and thermal transport with available experimental strategies. With a synergic pressure and doping strategy, we demonstrate from first principles that the bandgap of α -MgAgSb enlarges and its electrical and thermal transport can be decoupled. From the perspective of lattice dynamics, the locally vibrating three-centered Mg-Ag-Sb bonds generate multiple low-lying optical phonons which contribute large scattering channels among heat-carrying phonons and thus result in a strong anharmonicity. Under hydrostatic pressure from ambient to 50 GPa, the chemical bonds are strengthened and low-lying optical phonons move upward, which reduces the anharmonic three-phonon scattering events and thus increases lattice thermal conductivity. Under hydrostatic pressure, α -MgAgSb maintains high mechanical stability even at 550 K and 50 GPa, as verified by first-principles molecular dynamics simulations. By combining the pressure and the doping strategy to engineer density of states near the Fermi level, the thermoelectric power factor can be tuned to be significantly high while the thermal conductivity remains reasonably low. The physical insights gained from this work pave the way for decoupling electrical and thermal transport of α -MgAgSb via the synergic pressure and doping strategy toward improving its thermoelectric performance.

Published under license by AIP Publishing. https://doi.org/10.1063/1.5090456

I. INTRODUCTION

Thermoelectric (TE) technology holds great promise in advancing future energy utilization for its capability of directly converting a temperature gradient into electricity and vice versa. ¹⁻⁶ As the core of a TE module, high-performance TE materials have been extensively exploited to achieve high TE conversion efficiency. From a material's perspective, the performance of TE material is determined by the dimensionless number called figure of merit $ZT = S^2 \sigma T / (\kappa_{el} + \kappa_{lat})$, where S is the Seebeck coefficient, σ is the electrical conductivity, T is the absolute temperature, and κ_{el} and κ_{lat} are the electronic and lattice components of thermal conductivity, respectively. Historically, following Slack's "electron-crystal phonon-glass" concept, ⁷ two basic approaches are widely applied to improve ZT via either increasing

the power factor (PF) $S^2\sigma$ or decreasing κ_{lat} . Great endeavors, such as band engineering by introducing resonant states close to band edge, $^{8-10}$ pressure, 11,12 modulation doping, 13,14 and quantum confinement, 15,16 have been made to increase PF. On the other hand, hierarchical architectures, 17,18 doping, 19,20 point defects, 21,22 and dislocations 23,24 are widely applied to scatter heat-carrying phonons and thus reduce κ_{lat} . Yet, the remaining challenge, which is more fundamental, lies in the fact that PF and κ_{el} are strongly interdependent, which requires a revolutionary strategy to reach a delicate balance between them and then optimize ZT.

Recently, room-temperature thermoelectrics (ambient to 200 °C) have grown rapidly with the increasing demands for domestic applications. $^{25-27}$ However, the lack of high-ZT TE materials near room temperature has become a bottleneck. Ever since the first

^{a)}Author to whom correspondence should be addressed: hu@sc.edu

reported ZT value of ~ 0.35 at room temperature, 28 α -MgAgSb has drawn wide attention and become a promising candidate for room-temperature TE materials. High ZT values of ~1.1-1.4 near room temperature have been experimentally reported, and α-MgAgSb-based materials have better thermoelectric performance comparable to the commercial p-type Bi₂Te₃-based alloys.²⁹ Moreover, constituting of nontoxic and relatively low-cost elements makes α-MgAgSb more suitable for commercial applications. To further improve ZT of α -MgAgSb, it is essential to understand its lattice structure, electrical and thermal transport, and, in particular, how to decouple them. α-MgAgSb has a Nowotny-Juza phase and belongs to the class of "filled tetrahedral structures." 33 In α-MgAgSb, global and local weak chemical bonds coexist due to the distorted rocksalt lattice of Sb and Mg atoms. After performing lattice dynamics analysis, Ying et al.34 stated that the hierarchical chemical bonds of α -MgAgSb led to the ultralow κ_{lat} at room temperature. As for the electrical transport, Miao et al.35 showed that α-MgAgSb experienced a semimetal-semiconductor phase transition under hydrostatic pressure and its thermoelectric PF was greatly improved via the pressure and doping strategy by applying first-principles simulations. Yet, the essential understanding on how the pressure and doping strategy influence the thermal transport of α -MgAgSb is lacking, which is crucial to obtain ZT with a higher accuracy.

Motivated by the idea of Ref. 35, we systematically investigate how the combination of the pressure and the doping strategy decouples the electrical and thermal transport in α-MgAgSb from first principles. By applying anharmonic lattice dynamics coupled with the phonon Boltzmann transport theory, we attribute the atomistic origins of ultralow κ_{lat} to a strong phonon anharmonicity, low phonon relaxation time, and average group velocity. The strong phonon anharmonicity originates from the existence of multiple low-lying optical phonons which participate in the anharmonic scattering, while the low average group velocity originates from a weak chemical bonding. On the other hand, under hydrostatic pressure from ambient to 50 GPa, the bandgap of α-MgAgSb enlarges and its thermoelectric S increases, but σ and κ_{el} decrease. By combining the pressure and the doping strategy to engineer density of states near the Fermi level, we show that PF can be significantly high and $\kappa_{el} + \kappa_{lat}$ is kept reasonably low.

II. COMPUTATIONAL METHODOLOGY

It is well known that the transport properties of solids are fundamentally determined by the quantum interactions among microscopic electrons and phonons. $^{36-38}$ For phonon transport in pure crystal, κ_{lat} is dominated by the anharmonic phonon–phonon scattering. Following the Boltzmann transport theory under relaxation time approximation (RTA), κ_{lat} is determined by 39,40

$$\kappa_{lat} = \frac{1}{N\Omega} \sum_{\mathbf{q}v} C_{\mathbf{q}v} v_{\mathbf{q}v}^2 \tau_{ph}(\mathbf{q}v), \tag{1}$$

where Ω is the volume of the unit cell, N is the total number of q points in the first Brillouin zone, and C_{qv} , v_{qv} , and τ_{ph} are the specific heat, phonon group velocity, and relaxation time for a qv

phonon mode, respectively. Within the scheme of three-phonon scattering, the lowest-order perturbation of phonon anharmonicity, τ_{ph} , is given by 41,42

$$1/\tau_{ph} = 1/N \left(\sum_{ph}^{+} \Gamma_{ph}^{+} + \sum_{ph}^{-} 1/2\Gamma_{ph}^{-} \right),$$
 (2)

where Γ^+ and Γ^- correspond to the phonon's absorption and emission process, respectively, and can be obtained by calculating the third-order interatomic force (relevant theory and computational details are provided in the supplementary material).

As for electrons, their transport properties are mainly determined by electronic band structure and electron–phonon interaction. Following the simple free gas model, the electrical conductivity (σ) quantifying electron transport capability is determined by⁴³

$$\sigma_{\alpha\beta}(\varepsilon) = \frac{1}{N_{\mathbf{k}}} \sum_{i,\mathbf{k}} \sigma_{0\alpha\beta}(i,\mathbf{k}) \frac{\delta(\varepsilon - \varepsilon_{i,\mathbf{k}})}{d\varepsilon},\tag{3}$$

where N_k is the total k-points sampled in the first Brillouin zone and $\sigma_{0\alpha\beta}$ is the conductivity tensor expressed as $e^2\tau_{el}u_\alpha u_\beta$. The physical quantity u is the electron group velocity and τ_{el} is the electron relaxation time dominated by electron–phonon interaction. Since there exists weak electron–phonon coupling in α -MgAgSb, 13 we approximate τ_{el} as 10 fs in this work. Such an approximation can be verified by the overall agreement of theoretically calculated PF with the literature experiment. Under different doping concentrations and hydrostatic pressures, τ_{eb} and its energy dependence will change correspondingly. Yet, it would require huge computational cost to directly calculate the energy-dependent τ_{el} by performing electron–phonon calculations, and, therefore, in this work, we ignore the influence of doping and pressure on τ_{el} and assume it to be a constant. After obtaining $\sigma_{\alpha lb}$, κ_{el} is calculated as 43

$$\kappa_{el} = 1/(e^2 T\Omega) \int \sigma_{\alpha\beta}(\varepsilon)(\varepsilon - \mu)[-\partial f_{\mu}(T; \varepsilon)/\partial \varepsilon] d\varepsilon - TS^2 \sigma, \quad (4)$$

where T is the absolute temperature, μ is the chemical potential, S is the Seebeck coefficient, and f is the Fermi–Dirac distribution statistics of electrons.

III. RESULTS AND DISCUSSION

A. Mechanical stability

Prior to engineering phononic and electronic transport, it is essential to investigate the mechanical stability of α -MgAgSb under high hydrostatic pressure. By calculating the state of equation, Miao *et al.*³⁵ showed that α -MgAgSb is stable up to 55 GPa, though a semimetal–semiconductor transition occurs at a higher hydrostatic pressure. As presented in Fig. 1, the phonon dispersion curves and projected density of states (PDOS) of α -MgAgSb under high pressures up to 50 GPa show no imaginary phonon modes, indicating its lattice dynamical stability. To further rationalize its mechanical stability, we performed first-principles molecular dynamics

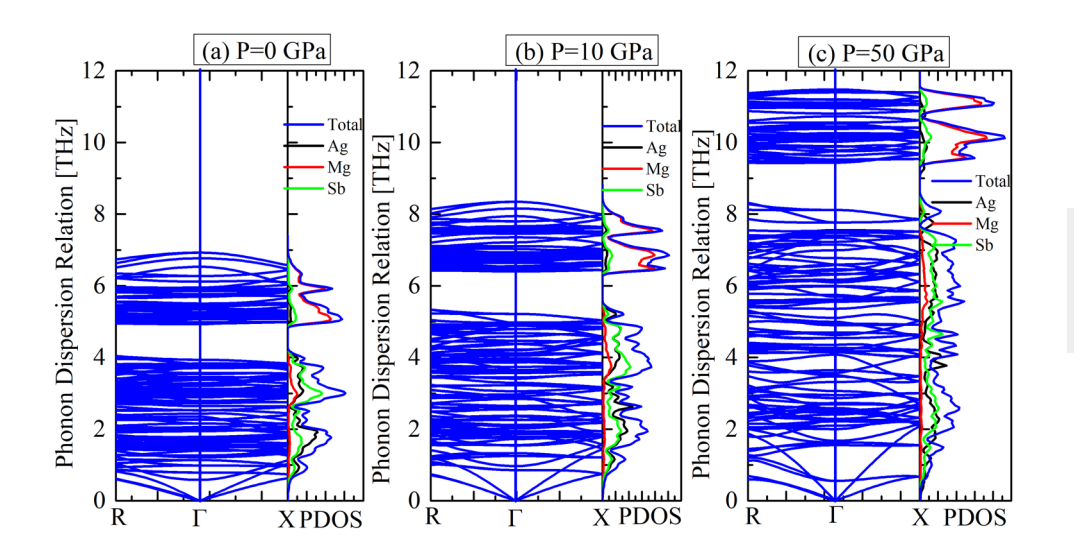


FIG. 1. The phonon dispersion relation and projected phonon density of states (PDOS) of α -MgAgSb under pressures of (a) 0 GPa, (b) 10 GPa, and (c) 50 GPa

(FPMD) simulations for α -MgAgSb under pressure of 50 GPa. By choosing a large supercell (384 atoms) and performing a 30 ps dynamic run (with a time step of 2 fs), we show that all element atoms of α -MgAgSb move randomly but still around their equilibrium positions even at 550 K, as indicated by the trajectory analysis of Fig. S1 in the supplementary material. Based on the FPMD simulations, Ying *et al.*³⁴ stated that the ultralow κ_{lat} of α -MgAgSb is inclined to the effects of phonon perspective, so we focus on analyzing κ_{lat} in the view of anharmonic phonon–phonon scattering.

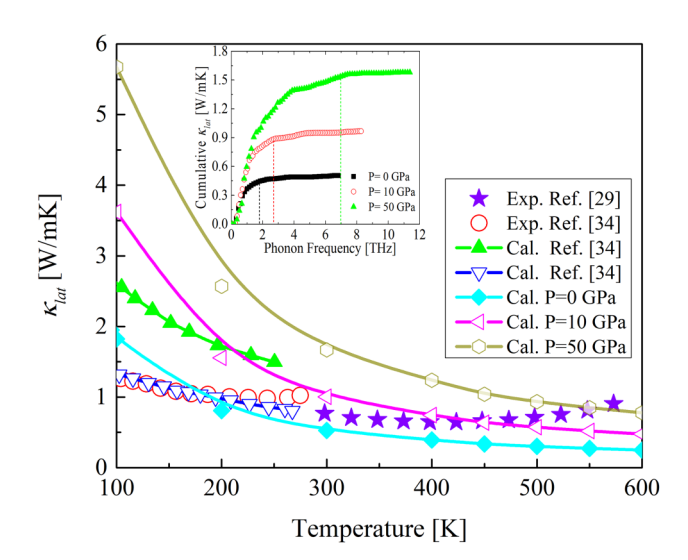


FIG. 2. The temperature-dependent lattice thermal conductivity (κ_{lat}) of $\alpha\textsc{-MgAgSb}$ under pressures varying from 0 to 50 GPa. The literature values from Refs. 29 and 34 are also plotted for comparison. (Inset) The comparison of cumulative of room temperature κ_{lat} vs phonon frequencies between different pressures.

B. Phonon transport

In Fig. 2, the calculated temperature-dependent κ_{lat} of α-MgAgSb under pressures up to 50 GPa is presented and it demonstrates overall agreement with the literature results.^{29,34} At 300 K, the calculated κ_{lat} of α -MgAgSb at 0 GPa is unprecedentedly low (0.58 W/mK), which agrees well with the measured value of $0.6\,W/mK^{29,32}$ but is relatively lower than that of Bi₂Te₃-based alloys. The experimental study showed that the small grain size and point defects were crucial to the ultralow κ_{lat} of α -MgAgSb. Yet, from first principles, it is difficult to quantify their contribution to thermal transport. Here, we deal with the pure α -MgAgSb crystal, neglect the influence of small grain size and point defects, and investigate the physics origin of its ultralow thermal conductivity. To interpret the ultralow κ_{lab} we first analyze the lattice anharmonicity and group velocity for the heat-carrying phonons. By analyzing the cumulative κ_{lat} , as shown in the inset of Fig. 2, the heat-carrying phonons of α -MgAgSb under 0 GPa lie in the frequency range of 0-2 THz and are extended to 0-7 THz under 50 GPa. From a phonon's perspective, the Grüneisen parameter γ_G is a measure of lattice anharmonicity and reflects the strength of phonon-phonon scattering, while the group velocity quantifies how fast phonons propagate and is mainly determined by the chemical bonding. In Fig. 3(a), we observe a high γ_G in α -MgAgSb under 0 GPa, with a maximum value of 2.3 at 2 THz and a weighted average of 1.36. The high γ_G suggests a strong phonon anharmonicity and a relatively low τ_{ph} (approximately 5 ps) for the heat-carrying phonons (see Fig. S2 in the supplementary material). Further analysis on the detailed scattering process suggests that the normal process predominates over the Umklapp process and mainly contributes to the total anharmonic phonon scattering. The anharmonic scattering among the heat-carrying phonons is predominated by the absorption process where two low-frequency phonons annihilate and one high-frequency optical phonon creates (see Fig. S3 in the supplementary material). On the other hand, the average group velocity of α-MgAgSb under 0 GPa is relatively low, as shown in Fig. 3(b), with a maximum value of 2.5 nm/ps at 1.2 THz.

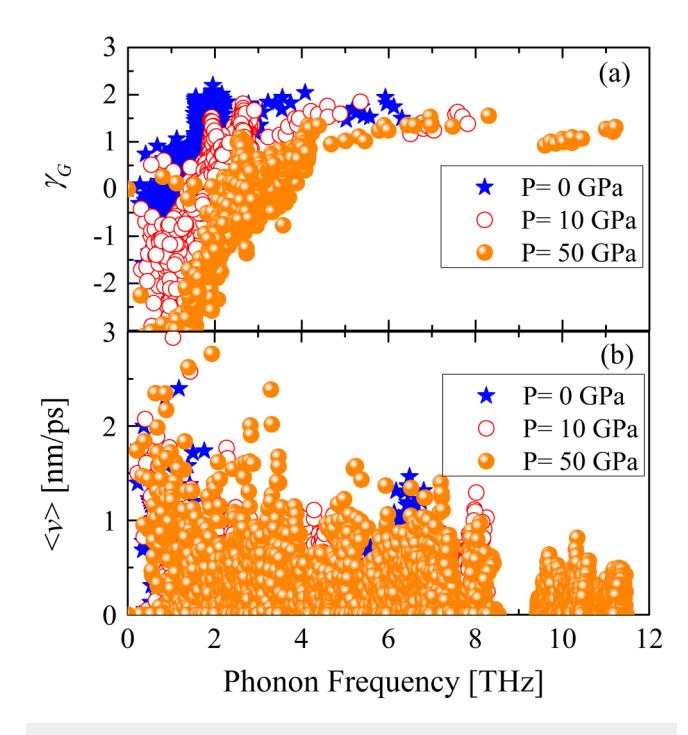


FIG. 3. The (a) frequency-dependent Grüneisen parameter (γ_G) and (b) averaged group velocity $\langle v \rangle$ vof α -MgAgSb at 300 K under pressures varying from 0 to 50 GPa.

C. Origin of strong phonon anharmonicity

Ying et al.³⁴ attributed the low κ_{lat} to the hierarchically weak chemical bonds in α -MgAgSb. The low group velocity originates from the global weak bonding, while the strong phonon anharmonicity is closely related to the locally vibrating three-centered Mg-Ag-Sb bonds. To verify this hypothesis, we calculate the charge density and chemical bonds of α -MgAgSb under pressures up to 50 GPa, as shown in Fig. 4. Under 0 GPa, the charge density is mainly bounded to Ag atoms and there is less overlap with that of

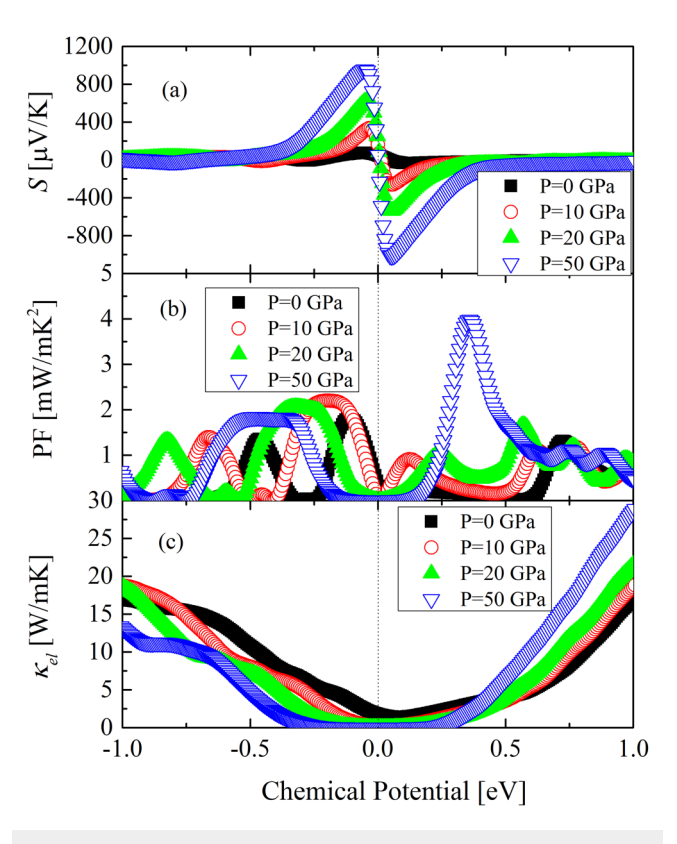


FIG. 5. The calculated (a) Seebeck coefficient (S), (b) power factor (PF), and (c) electronic thermal conductivity (κ_{el}) of α -MgAgSb at 300 K under pressures varying from 0 to 50 GPa.

Mg and Sb atoms, resulting in the low restoring forces for Ag atoms [Fig. 4(a)]. Since Ag atoms move in the polyhedral formed by the distorted rocksalt lattice of Mg and Sb atoms, the low restoring forces on Ag atoms induce multiple low-lying optical phonons. This can be verified by the projected PDOS which show that Ag

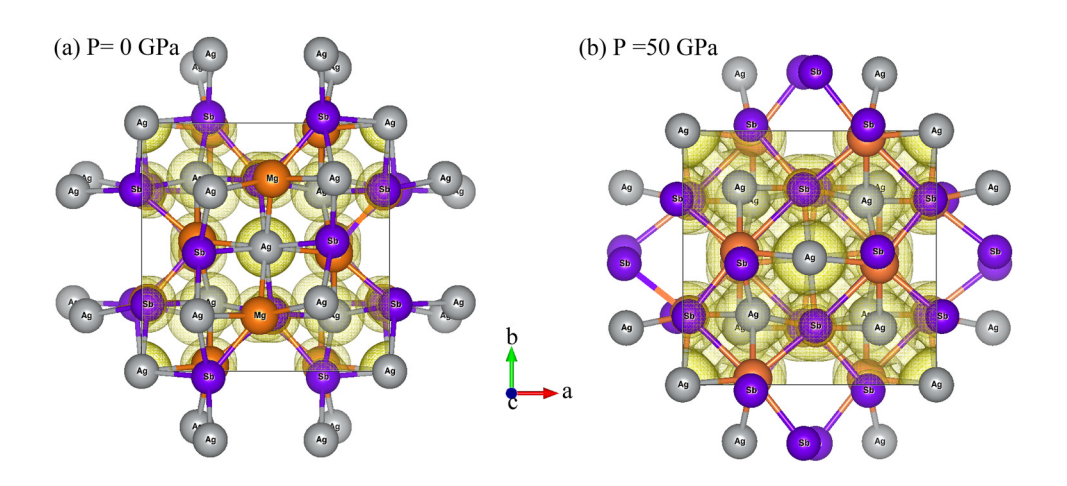


FIG. 4. The lattice structure, charge density, and chemical bonds of α -MgAgSb under pressures of (a) 0 GPa and (b) 50 GPa.

atoms mainly contribute to the low-lying phonon modes in α-MgAgSb. At a hydrostatic pressure of 50 GPa, the charge density of Ag, Mg, and Sb atoms increases and overlaps with each other, leading to the strong restoring forces [Fig. 4(b)]. Thus, the chemical bonds become shortened and strong. Under 0 GPa, the Mg-Ag, Mg-Sb, and Ag-Sb chemical bond lengths are 2.922 Å, 2.986 Å, and 2.905 Å, respectively, and reduce to 2.628 Å, 2.893 Å, and 2.597 Å under 50 GPa. Consequently, the distortion degree of the rocksalt lattice reduces and the low-lying optical phonons shift to higher frequencies, as shown in Fig. 1. Since the anharmonic scattering among the heat-carrying phonons is predominated by the absorption process such as acoustic + acoustic → optical [see Fig. S3(b) in the supplementary material], the upward move of the low-lying optical phonons certainly reduces the anharmonic scattering event and thus decreases γ_G . Meanwhile, the strengthened chemical bonds would lead to the increased group velocity and finally increases κ_{lat} , as shown in Fig. 2.

D. Electron transport

As chemical bonds strengthen under a hydrostatic pressure, the bandgap of α -MgAgSb increases, which is verified by theoretical calculations. The critical room-temperature Seebeck coefficient S increases slightly from 45 μ V/K under 0 GPa to 49.37 μ V/K under 50 GPa. However, as the bandgap opens, the relevant room-temperature electrical conductivity σ decreases tremendously from

 1.53×10^5 S/m under 0 GPa to 0.89 S/m under 50 GPa. Consequently, the room-temperature thermoelectric PF $S^2\sigma$ significantly reduces from 0.43 mW/mK^2 under 0 GPa to $2 \times 10^{-6} \text{ mW/mK}^2$ at 50 GPa, respectively. Thus, the pressure strategy alone cannot improve the thermoelectric performance of α -MgAgSb. Recently, the doping strategy has been experimentally verified to effectively improve ZT of α-MgAgSb.³⁰ Theoretical study also shows that the combined pressure and doping strategy can increase the PF by 110% at 550 K.35 Motivated by this study, we combine the pressure and doping strategy to manipulate the electronic transport properties. As presented in Fig. 5, the p-doping strategy can slightly increase S from $45 \mu V/K$ to $72.8\,\mu\text{V/K}$ by shifting the Fermi level down by 0.07 eV under 0 GPa. In contrast, under 50 GPa, the p-doping (n-doping) strategy significantly increases S from $50 \,\mu\text{V/K}$ to a maximum of $955 \,\mu\text{V/K}$ $(1015 \,\mu\text{V/K})$ by shifting the Fermi level down (up) by 0.05 eV, respectively. At such high doping, disorder concentration will increase and more electrons are localized mainly around the band edges, leading to an increase in the energy bandgap and thus the Seebeck coefficient. However, for heavy doping with more free carriers, S decreases smoothly with the Fermi level shift increasing. On the other hand, the doping strategy introduces more free carriers in the semiconducting α -MgAgSb and thus increases σ . By combining the pressure and doping strategy, the thermoelectric PF increases from 0.43 mW/mK² to 3.9 mW/mK², i.e., almost an order of magnitude augment. The substantial increase of PF originates from the engineered density of states near the Fermi level.³⁵ Yet, the enhanced PF is for a highly

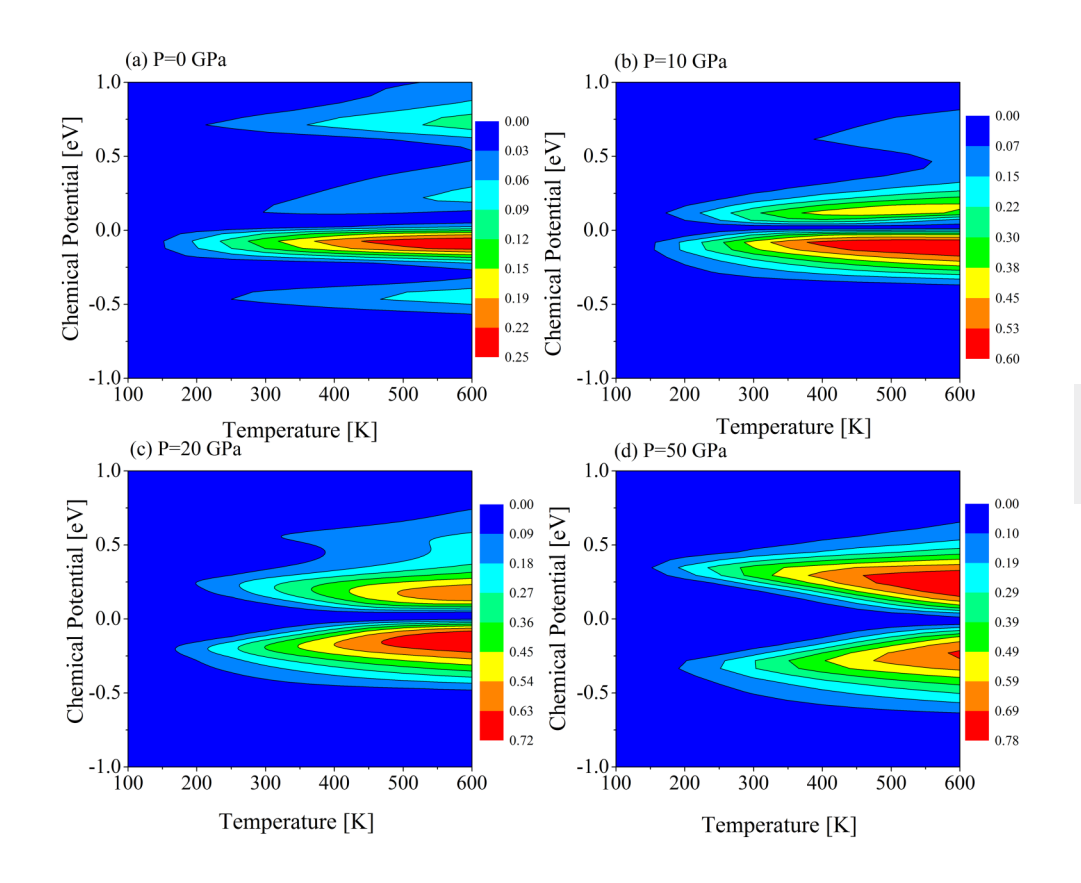


FIG. 6. Theoretically predicted ZT of α -MgAgSb at different temperatures and chemical potentials by the synergic pressure and the doping strategy.

disordered regime that may require a special set of experimental settings to realize. While applying the doping strategy, the introduced carriers will further scatter phonons and reduce κ_{lat} . Consequently, $\kappa_{el} + \kappa_{lat}$ will be kept reasonably low, while $S^2\sigma$ can be engineered significantly high, leading to the enhanced ZT as shown in Fig. 6. With the high doping concentration, the lattice contribution to thermal transport will be much smaller than the electronic part. Thus, ZT can be approximated as $S^2\sigma/\kappa_{eb}$ since the calculated σ and κ_{el} are proportional to τ_{el} . Then, the assumption of the constant value for τ_{el} will not affect the final value of ZT. Also, it is worth mentioning that the maximized ZT of 0.72 under 20 GPa is relatively smaller than 0.78 under 50 GPa. Considering that high pressure requires a higher cost to accomplish, the relatively lower pressure should be applied in practice.

IV. CONCLUSION

In summary, we examine from first-principles calculations the atomistic origins of electrical and thermal transport in α-MgAgSb and demonstrate how the combination of the pressure and the doping strategy decouples them to boost thermoelectric performance. Anharmonic lattice dynamics calculations determine an ultralow κ_{lat} of 0.58 W/mK at room temperature, in good agreement with experiments, which is caused by the strong phonon anharmonicity due to the existence of a large number of low-lying optical phonons and a weak chemical bonding. Under a hydrostatic pressure of up to 50 GPa, the chemical bonds are strengthened and low-lying optical phonons have an upward shift, leading to the weakened anharmonic scattering and the slightly increased κ_{lat} . However, by combining the doping strategy to engineer energy states near the Fermi level, the thermoelectric PF can be engineered significantly high to be 3.9 mW/mK², which compensates the minor increase in lattice thermal conductivity, with the other key quantity of electronic thermal conductivity remaining reasonably low. This work mainly contributes to uncovering the physical insights into how the synergic pressure and the doping strategy decouples the electrical and thermal transport in α-MgAgSb.

SUPPLEMENTARY MATERIAL

See the supplementary material for the computational details, the relevant theory about anharmonic lattice dynamics, and the first-principles molecular dynamics trajectory of α -MgAgSb under hydrostatic pressures.

ACKNOWLEDGMENTS

J.-Y.Y. is grateful for the financial support by the grant supported by Shandong University (Qilu Young Scholar 89963031) and the Excellence Initiative of the German federal and state governments (Project No. StUpPD_268-17). W. Zhang thanks support from the Shandong Provincial Natural Science Foundation, China (No. ZR2017BEE051). We gratefully acknowledge computing time granted by the John von Neumann Institute for Computing (NIC) and provided on the supercomputer JURECA at Forschungszentrum Jülich, Germany (Project ID: JHPC51). Research reported in this publication was supported in part by the National Science Foundation (NSF) and SC EPSCoR/IDeA

Program under National Science Foundation (NSF) Award Nos. OIA-1655740 and SC EPSCoR/IDeA 19-SA06.

REFERENCES

¹B. C. Sales, Science **295**, 1248 (2002).

²H. J. Goldsmid and R. W. Douglas, Br. J. Appl. Phys. 5, 458 (1954).

³B. Poudel, Q. Hao, Y. Ma, Y. Lan, A. Minnich, B. Yu, X. Yan, D. Wang, A. Muto, D. Vashaee, X. Chen, J. Liu, M. S. Dresselhaus, G. Chen, and Z. Ren, Science 320, 634 (2008).

⁴D. Kraemer, B. Poudel, H.-P. Feng, J. C. Caylor, B. Yu, X. Yan, Y. Ma, X. Wang, D. Wang, A. Muto, K. McEnaney, M. Chiesa, Z. Ren, and G. Chen, Nat. Mater. 10, 532 (2011).

⁵H. Goldsmid, Thermoelectric Refrigeration (Springer, 2013).

⁶D. M. Rowe, Conversion efficiency and figure-of-merit, in CRC Handbook of Thermoelectrics (CRC Press, 1995), p. 31.

⁷G. A. Slack, MRS Online Proc. Libr. Arch. 478, 47 (1997).

⁸J. P. Heremans, V. Jovovic, E. S. Toberer, A. Saramat, K. Kurosaki, A. Charoenphakdee, S. Yamanaka, and G. J. Snyder, Science 321, 554 (2008).

⁹Q. Zhang, B. Liao, Y. Lan, K. Lukas, W. Liu, K. Esfarjani, C. Opeil, D. Broido, G. Chen, and Z. Ren, Proc. Natl. Acad. Sci. 110, 13261 (2013).

10Y. Pei, X. Shi, A. LaLonde, H. Wang, L. Chen, and G. J. Snyder, Nature 473, 66 (2011).

¹¹G. A. Slack and R. G. Ross, J. Phys. C Solid State Phys. 18, 3957 (1985).

¹²Y. Zhang, X. Jia, H. Sun, B. Sun, B. Liu, H. Liu, L. Kong, and H. Ma, J. Alloys Compd. 667, 123 (2016).

¹³Z. Liu, Y. Wang, J. Mao, H. Geng, J. Shuai, Y. Wang, R. He, W. Cai, J. Sui, and Z. Ren, Ad. Energy Mater. 6, 1502269 (2016).

¹⁴J. Mao, J. Shuai, S. Song, Y. Wu, R. Dally, J. Zhou, Z. Liu, J. Sun, Q. Zhang, C. dela Cruz, S. Wilson, Y. Pei, D. J. Singh, G. Chen, C.-W. Chu, and Z. Ren, Proc. Natl. Acad. Sci. U.S.A. 114, 10548 (2017).

¹⁵D. Parker, X. Chen, and D. J. Singh, *Phys. Rev. Lett.* **110**, 146601 (2013).

16L. Hicks and M. S. Dresselhaus, Phys. Rev. B 47, 12727 (1993).

¹⁷K. Biswas, J. He, I. D. Blum, C.-I. Wu, T. P. Hogan, D. N. Seidman, V. P. Dravid, and M. G. Kanatzidis, Nature 489, 414 (2012).

¹⁸L.-D. Zhao, V. P. Dravid, and M. G. Kanatzidis, Energy Environ. Sci. 7, 251 (2014).

19 A. J. Minnich, M. S. Dresselhaus, Z. F. Ren, and G. Chen, Energy Environ. Sci. 2, 466 (2009).

²⁰J. Shuai, J. Mao, S. Song, Q. Zhu, J. Sun, Y. Wang, R. He, J. Zhou, G. Chen, and D. J. Singh, Energy Environ. Sci. 10, 799 (2017).

²¹J.-Y. Yang, L. Cheng, and M. Hu, Appl. Phys. Lett. 111, 242101 (2017).

²²Z. Liu, H. Geng, J. Mao, J. Shuai, R. He, C. Wang, W. Cai, J. Sui, and Z. Ren, J. Mater. Chem. A 4, 16834 (2016).

²³D. Kotchetkov, J. Zou, A. A. Balandin, D. I. Florescu, and F. H. Pollak, Appl. Phys. Lett. **79**, 4316 (2001).

²⁴D. Li, H. Zhao, S. Li, B. Wei, J. Shuai, C. Shi, X. Xi, P. Sun, S. Meng, and L. Gu, Adv. Funct. Mater. 25, 6478 (2015).

25 Y. Wu, R. Zhai, T. Zhu, and X. Zhao, Mater. Today Phys. 2, 62 (2017).

²⁶R. Venkatasubramanian, E. Silvola, T. Colpitts, and B. O'quinn, *Materials for Sustainable Energy: A Collection of Peer-Reviewed Research and Review Articles from Nature Publishing Group* (World Scientific, 2011), p. 120.

from Nature Publishing Group (World Scientific, 2011), p. 120.

27G. J. Snyder and E. S. Toberer, Materials for Sustainable Energy: A Collection of Peer-Reviewed Research and Review Articles from Nature Publishing Group (World Scientific, 2011), p. 101.

28M. J. Kirkham, A. M. dos Santos, C. J. Rawn, E. Lara-Curzio, J. W. Sharp, and

M. J. Kirkham, A. M. dos Santos, C. J. Rawn, E. Lara-Curzio, J. W. Sharp, and A. J. Thompson, Phys. Rev. B 85, 144120 (2012).

²⁹H. Zhao, J. Sui, Z. Tang, Y. Lan, Q. Jie, D. Kraemer, K. McEnaney, A. Guloy, G. Chen, and Z. Ren, Nano Energy 7, 97 (2014).

³⁰Z. Liu, J. Mao, J. Sui, and Z. Ren, Energy Environ. Sci. **11**, 23 (2018).

³¹ Z. Liu, Y. Wang, W. Gao, J. Mao, H. Geng, J. Shuai, W. Cai, J. Sui, and Z. Ren, Nano Energy 31, 194 (2017).

- ³⁸Z. Tong and H. Bao, Int. J. Heat Mass Transf. 117, 972 (2018).
- 39D. A. Broido, M. Malorny, G. Birner, N. Mingo, and D. A. Stewart, Appl. Phys. Lett. **91**, 231922 (2007).

 ⁴⁰H. Bao, J. Chen, X. Gu, and B. Cao, ES Energy Environ. **1**, 16 (2018).
- 41 W. Li, J. Carrete, N. A. Katcho, and N. Mingo, Comput. Phys. Commun. **185**, 1747 (2014).
- ⁴²W. Li and N. Mingo, Phys. Rev. B **89**, 184304 (2014).
- 43B. Liao, J. Zhou, B. Qiu, M. S. Dresselhaus, and G. Chen, Phys. Rev. B 91, 235419 (2015).

³²P. Ying, X. Liu, C. Fu, X. Yue, H. Xie, X. Zhao, W. Zhang, and T. Zhu, Chem. Mater. 27, 909 (2015).

³³ T. Graf, C. Felser, and S. S. Parkin, Prog. Solid State Chem. 39, 1 (2011).

³⁴P. Ying, X. Li, Y. Wang, J. Yang, C. Fu, W. Zhang, X. Zhao, and T. Zhu, Adv. Funct. Mater. 27, 1604145 (2017).

³⁵ N. Miao, J. Zhou, B. Sa, B. Xu, and Z. Sun, Appl. Phys. Lett. 108, 213902 (2016). 36 J.-Y. Yang, G. Qin, and M. Hu, Appl. Phys. Lett. 109, 242103 (2016).

³⁷J.-Y. Yang, S.-Y. Yue, and M. Hu, Phys. Rev. B 94, 235153 (2016).